JPET Fast Forward. Published on October 1, 2018 as DOI: 10.1124/jpet.118.248997
This article has not been copyedited and formatted. The final version may differ from this version.

TITLE PAGE

Title:

Targeting Canine *KIT* Promoter by Candidate DNA G-quadruplex Ligands

Authors:

Eleonora Zorzan, Silvia Da Ros, Mery Giantin, Lara Zorro Shahidian[1], Giorgia Guerra, Manlio Palumbo, Claudia Sissi, and Mauro Dacasto

Authors affiliations:

Department of Comparative Biomedicine and Food Science, University of Padua, Agripolis Legnaro, Padua, Italy (E.Z., M.G., L.Z.S., G.G., M.D.); and Department of Pharmaceutical and Pharmacological Sciences, University of Padua, Padua, Italy (S.D.R., M.P., C.S.)

RUNNING TITLE PAGE

Running title:

Dog *KIT* Promoter and G4 Ligands

Corresponding authors:

Prof. Mauro Dacasto, DVM, PhD, Dipl. ECVPT, Department of Comparative Biomedicine and Food Science, Division of Veterinary Pharmacology and Toxicology, University of Padua, viale dell'Università 16, I-35020 Agripolis Legnaro (Padua), Italy; Tel.: +39.049.827.2935; fax: +39.049.827.2973; email: mauro.dacasto@unipd.it

Prof. Claudia Sissi, MSc (Pharmacy and Industrial Pharmacy), PhD, Department of Pharmaceutical and Pharmacological Sciences, University of Padua, Padua, Italy; via Marzolo 5, I-35131 Padua, Italy; Tel.: +39.049.827.5711; fax: +39.049.827.5366; email: claudia.sissi@unipd.it

Number of text pages: 43

Number of tables: 2

Number of figures: 10

Number of references: 51

Number of words in the Abstract: 250

Number of words in the Introduction: 750

Number of words in the Discussion: 1375

JPET Fast Forward. Published on October 1, 2018 as DOI: 10.1124/jpet.118.248997
This article has not been copyedited and formatted. The final version may differ from this version.

Nonstandard abbreviation used:

ANOVA, analysis of variance; *ATP5β*, ATP synthase, H^+ transporting, mitochondrial F1 complex, beta polypeptide; AU, arbitrary units; *BCL2*, B-cell leukemia/lymphoma 2; *CGI-119*, transmembrane BAX inhibitor motif containing 4; *CCZ1*, vacuolar protein trafficking and biogenesis associated homolog; *KIT*, v-kit Hardy-Zuckerman 4 feline sarcoma viral oncogene homolog; DMSO, dimethyl sulfoxide; E, efficiency; EC_{50}, half maximal effective concentration; G4, G-quadruplex; *GAPDH*, glyceraldehyde 3-phosphate dehydrogenase; *GOLGA1*, Golgin A1; IC_{50}, half maximal inhibitory concentration; ICG, internal control gene; *KRAS*, Kirsten rat sarcoma viral oncogene homolog; MCT, mast cell tumor; MDCK, Madin-Darby Canine Kidney; *MYC*, v-myc avian myelocytomatosis viral oncogene homolog; qPCR, quantitative real-time PCR; RQ, relative quantification; Sp1, specific protein 1; S.D., standard deviation; T, time; *TERT*, telomerase reverse transcriptase; TKI, tyrosine kinase inhibitor; TSS, transcription starting site; TO, thiazole orange; *VEGFA*, vascular endothelial growth factor A; UPL, Universal Probe Library.

Section assignment

Drug Discovery and Translational Medicine

JPET Fast Forward. Published on October 1, 2018 as DOI: 10.1124/jpet.118.248997
This article has not been copyedited and formatted. The final version may differ from this version.

ABSTRACT

G-quadruplexes (G4) are nucleic acid secondary structures frequently assumed by G-rich sequences located mostly at telomeres and proto-oncogenes promoters. Recently, we identified, in canine *KIT* promoter, two G-rich sequences able to fold into G4: d_kit1 and d_kit2_A16. In this study, an anthraquinone (AQ1) and an anthracene derivative (AN6), known to stabilize the G4 structures of the corresponding human h_kit1 and h_kit2, were tested on the canine G4 and in two canine mast cell tumor (MCT) cell lines (C2 and NI-1) to verify their capability to downregulate *KIT* expression. The cytotoxicity of AQ1 and AN6 was determined using the Alamar Blue test; meantime, the constitutive expression of *KIT* and other proto-oncogenes containing G4 structures in their promoter (*BCL2, VEGFα, VEGFR2, KRAS,* and *TERT*) was assessed by quantitative real-time PCR (qPCR). Then, the time- and dose-dependent effects of both ligands on target gene expression were assessed by qPCR. All target genes were constitutively expressed up to 96 hours of culture. Both ligands decreased *KIT* mRNA levels and c-kit protein amount, and AN6 was comparatively fairly more effective. DNA interaction studies and a dual-luciferase gene reporter assay performed on a non-cancerous canine cell line (MDCK) proved that this downregulation was the result of the interaction of AN6 with *KIT* proximal promoter. Interestingly, present results only partially overlap with former ones previously obtained in human cell lines, where AQ1 was found as the most effective compound. These preliminary data might suggest AN6 as a promising candidate for the selective targeting of canine *KIT*-dependent tumors.

INTRODUCTION

The G-quadruplex (G4) are tetrahelical structures formed by guanine-rich nucleic acid sequences. In these structural elements, four guanine residues are connected through Hoogsteen hydrogen bonds to constitute a G-quartet, and three or more quartets stacked one over the other form a G4 (Zhao et al., 2007; Lipps and Rhodes, 2009). Bioinformatics analysis identified around 400,000 putative G4-forming sequences in the human genome (Bidzinska et al., 2013), preferentially localized to telomeres and functional regions such as the transcription start site, the 5'-UTR, and the 5' end of the first intron; however, they are depleted in coding regions (Huppert and Balasubramanian, 2007; Maizels and Gray, 2013; Rhodes and Lipps, 2015). Evidences suggest that G4 formation plays a role in cellular telomerase maintenance, DNA transcription and RNA translation (Huppert and Balasubramanian, 2007; Bidzinska et al, 2013; Teng et al., 2017).

The sequence of these guanine-rich portions are generally highly conserved between different species, suggesting a selection pressure to retain such sequences at specific genomic sites (Lipps and Rhodes, 2009). This conservation is greatest among mammalian species, while it decreases in non-mammalian species and other organisms (Lipps and Rhodes, 2009). The presence of G4-forming sequences in genomes other than the human one has already been investigated, particularly in prokaryotes (Kang and Henderson, 2002; Rawal et al., 2006; Beaume et al., 2013; Kota et al., 2015) and warm-blooded animals such as chicken, rat, mouse, dog and zebrafish (Du et al., 2007; Zhao et al., 2007; Verma et al., 2008). Likewise to humans, the maximum frequency of putative G4-forming DNA sequences occurs in the gene transcriptional regulatory region, usually comprised between the -500 and +499 region, and particularly in the 100 bp preceding the transcription starting site (Zhao et al., 2007).

Recently, three G4-forming structures (h_kit1, h_kit2 and kit*) have been identified in the proximal promoter of the human proto-oncogene v-kit Hardy-Zuckerman 4 feline sarcoma

viral oncogene homolog (*KIT*; Rankin et al., 2005; Fernando et al., 2006; Raiber et al., 2012). *KIT* codes for a tyrosine kinase receptor (c-kit) implicated in cell survival, proliferation and differentiation; furthermore, the occurrence of activating mutations and/or its overexpression can result in aberrant functions and oncogenic cellular transformation in cells such as interstitial cells of Cajal and myeloid cells (Balasubramanian et al., 2011). The stabilization of human *KIT* G4 has been induced by using different classes of G4 ligands, such as trisubstituted isoalloxazines, bis-indole carboxamides, and benzo[a]phenoxazines; in all instances, a reduction of gene expression was derived (Bejugam et al., 2007; Dash et al., 2008; McLuckie et al., 2011). In a previous study, we selected and tested in different human neoplastic cell lines an anthraquinone and an anthracene derivative (AQ1 and AN6, respectively). Both compounds stabilized h_kit1 and h_kit2 and led to an inhibition of cell proliferation and *KIT* downregulation, with AQ1 being more effective than AN6 (Zorzan et al., 2016).

Pet dogs spontaneously develop cancers that share many characteristics with those found in humans, including biochemical pathways known to be drivers in certain human malignancies; this offers to comparative oncologists the opportunity to target these mechanisms in dogs and allow an accurate preclinical assessment of novel therapeutics (Gardner et al., 2016).

In canines, cutaneous mast cell tumor (MCT) is the most common skin tumor and *KIT* mutations cause a constitutive protein activation resulting in an uncontrolled mast cell proliferation (Gil da Costa, 2016). The advent of target therapy, and particularly the use of tyrosine kinase inhibitors (TKIs) brought some benefits in MCT therapeutic approach; however, the potential for drug-resistance phenomena and the need to choose the best anticancer drug according to *KIT* mutational profile represent common problems (London et al., 2009; Bonkobara, 2015).

By a sequencing work, we confirmed that also canine *KIT* promoter presents two putative G4 sequences: d_kit1 and d_kit2. The former is highly conserved between human and dog, while the second is species-specific and present a further isoform named d_kit2_A16. Accordingly, h_kit1 and d_kit1 share the same structural properties, whereas some differences in terms of folding kinetic and population distribution were observed between h_kit2 and d_kit2 (Da Ros et al., 2014).

With the aim to validate the *KIT* proximal promoter of dogs as a pharmacological target for the prevention of malignant cell proliferation, in the present study we compared the interaction of AQ1 and AN6 with the human and canine kit1 and kit2 and, subsequently, we tested the two derivatives on two canine MCT cell lines (C2 and NI-1) already used in TKIs validation (Dubreuil et al., 2009; Hadzijusufovic et al., 2012; Halsey et al., 2014).

MATERIALS AND METHODS

Ligands. AQ1 and AN7 were synthesized by Prof. G. Zagotto (University of Padua, Italy). Stock solutions were prepared as previously reported (Zorzan et al., 2016).

Canine cell lines. Two canine MCT cell lines were used in the present study. The former one (C2 cell line) is a well-characterized canine MCT cell line, expressing a mutated *KIT* genotype (48 bp internal tandem duplication in the juxtamembrane domain); this cell line is the most commonly used in *in vitro* studies on canine MCT and was kindly provided by Dr. Patrice Dubreuil (Centre de Recherche en Cancérologie de Marseille, France). The second one (NI-1 cell line), is a most recent canine MCT cell line, expressing a mutated *KIT* genotype (107C>T; 1187A>G; $ITD^{1263\text{-}1275}$) and kindly provided by Prof. Peter Valent (Medizinische Universität Wien, Austria) and Drs. Emir Hadzijusufovic and Michael Willmann (Veterinärmedizinische Universität Wien, Austria). This second cell line was essentially used for confirmatory studies. Cells were cultured in RPMI 1640 medium supplemented with 10% fetal bovine serum (FBS), 2 mM L-glutamine, 1 mM sodium pyruvate, and 1% penicillin/streptomycin (Gibco, Thermo Fisher Scientific, Waltham, MA, USA). The Madin-Darby Canine Kidney (MDCK) cell line was purchased from the European Collection of Cell Cultures (ECACC, Salisbury, UK). Cells were cultured in EMEM supplemented with 10% FBS, 2 mM L-glutamine, 1% non-essential amino acids (NEAA, Gibco, Thermo Fisher Scientific, Waltham, MA, USA), and 1% penicillin/streptomycin. Cell number and viability were checked by using the Trypan Blue dye exclusion test (Sigma-Aldrich Co., St. Louis, USA). Furthermore, cell cultures were screened routinely for *Mycoplasma spp.* contamination using the PCR Mycoplasma Test Kit (PromoKine, Heidelberg, Germany) as per manufacturer's instructions. For all the experiments, cells were used in passages comprised between 5-30 maximum.

JPET Fast Forward. Published on October 1, 2018 as DOI: 10.1124/jpet.118.248997
This article has not been copyedited and formatted. The final version may differ from this version.

Sequencing of *KIT* proximal promoter. C2 and NI-1 cells were used to amplify (PCR) and clone into TOPO TA vector the canine *KIT* proximal promoter (KF471023), according to Da Ros et al. (2014). The plasmid DNA from eight different colonies was sequenced.

Fluorometric titration and Fluorescent Intercalator Displacement (FID) assay. Fluorometric measurements were performed using a Perkin Elmer LS55 Luminescence Spectrometer equipped with a Haake DC 30 (power supply) and K20 (bath) to thermostat cell holder. Spectra were acquired using a quartz cuvette with 10 mm path length and the following parameters: emission range 520-680 nm; excitation wavelength 501 nm; scanning speed 120 nm/min; 25 °C. For FID assay, a solution containing 0.62 µM of target DNA and 1.24 µM of thiazole orange (TO) was added of increasing concentrations of tested ligand in 10 mM Tris, 50 mM KCl, pH 7.4. Changes in fluorescence emission were recorded. The percentage of TO displacement was calculated as follows: TO displacement = 100 - [(F/F_0) × 100], where F_0 is the fluorescence before addition of the ligand, plotted as a function of compound concentration. From these plots the EC_{50} (half maximal effective concentration) was calculated. Each titration was repeated at least in triplicate.

Fluorescence melting studies. Fluorescence melting analyses were performed with Light Cycler® 480 II (Roche Applied Science, Indianapolis, IN, USA), by setting the excitation source at 488 nm and recording the fluorescence emission at 520 nm. Before data acquisition, a solution containing 0.25 µM DNA in 10 mM LiOH, pH 7.5 (H_3PO_4) with 50 mM KCl was loaded on each well of a 96-well plate and then added with increasing concentrations of the tested ligand. Samples were first heated to 95 °C at a rate of 0.1 °C s^{-1}, maintained at 95 °C for 5 min and then annealed by cooling to 30 °C at a rate of 0.1 °C s^{-1}. Subsequently, samples were maintained at 30 °C for 5 min before being slowly heated to 95 °C (1 °C min^{-1}) and annealed at a rate of 1 °C min^{-1}. For the analyses with double strands oligonucleotides, the two complementary strands were previously annealed ON in 10 mM

JPET Fast Forward. Published on October 1, 2018 as DOI: 10.1124/jpet.118.248997
This article has not been copyedited and formatted. The final version may differ from this version.

LiOH, pH 7.5 with H_3PO_4. Then, samples were slowly heated to 95 °C (1 °C min^{-1}) and annealed at a rate of 1 °C min^{-1}. For all analyses, recordings were taken during both these melting and annealing steps to check for hysteresis. Melting temperatures were determined from the first derivatives of the melting profiles using the Roche LightCycler software. Each curve was repeated at least three times and errors were ± 0.4 °C.

Polymerase stop assay. The assay was performed using a primer (d[TA_2TACGACTCACTATAG]) previously labelled at the 5'-terminal with ^{32}P. Template strands were design to contain the target sequences (here named X) at conserved position (d[TC_2A_2CTATGTATAC(X)ACATATCGATGA_3T_2GCTATAGTGAGTCGTAT$_2$A]. For the annealing phase, a solution of 2:1 labeled primer:template was prepared in 10 mM Tris pH 7.5 and 50 mM KCl. The mixture was kept for five minutes at 95 °C and then left to slowly cool down at room temperature. For primer extension step, the above solution was added of 2.5 U *Taq* DNA Polymerase (Thermo Fisher Scientific, Waltham, MA, USA), of increasing ligand concentrations (0.1 – 10 μM) as well as of $MgCl_2$ (3 mM) and dNTPs (100 μM). The resulting mixture was kept at 55 °C for 30 minutes, cooled in ice, dried and finally solubilized with 5 μL of loading buffer (80% formamide in water with 1% bromophenol blue and xylene cyanol). Before loading on the gel, samples were put on boiling water for 5 minutes and then directly on ice. The reaction products were resolved on a 20% polyacrylamide gel (acrylamide: bis-acrylamide 19:1) with 7 M urea in 1X TBE buffer (89 mM Tris base, 89 mM boric acid, 20 mM Na_2EDTA). At the end of the electrophoretic run, the gel was exposed overnight on a storage phosphor screen (Amersham Pharmacia Biotech Italia, Milan, Italy) and finally scanned with a Storm 840 (Amersham Pharmacia Biotech Italia, Milan, Italy).

G4 ligands cytotoxicity. C2 and NI-1 cells were seeded in 96-wells plates at a concentration of 2 x 10^4 cells per well and treated with AQ1 and AN6 at concentrations comprised between 0.01 μM and 10 μM. Additional wells, either exposed to the vehicle

JPET Fast Forward. Published on October 1, 2018 as DOI: 10.1124/jpet.118.248997
This article has not been copyedited and formatted. The final version may differ from this version.

(dimethyl sulfoxide, DMSO, 0.1% final concentration) or containing the medium only were included in each experiment, too. After 72 hours of exposure, the G4 ligands cytotoxicity was measured by adding to each well 20 µL of CellTiter-Blue® Cell Viability Assay solution (Alamar Blue, Promega, Madison, USA) and measuring the fluorescence at 560 nm (excitation wavelength) and 590 nm (emission wavelength) by using a VICTOR™X4 Multilabel Plate Reader (Perkin Elmer, Waltham, USA). Three separate experiments were executed, and each concentration was tested in sestuplicate.

Time-dependent constitutive expression of target genes. Constitutive mRNA levels of six genes containing putative G4 structures in their promoter were measured in C2 and NI-1 cells seeded onto 6-well plates at a final concentration of 6 x 10^5 cells/well and collected after 6, 24, 48, 72 and 96 hours (T_6, T_{24}, T_{48}, T_{72}, T_{96}, respectively). Cell pellets were washed once with PBS 1X containing 0.02% EDTA and, finally, resuspended in 0.5 mL of TRIzol® reagent (Thermo Fisher Scientific, Waltham, MA, USA). Total RNA extraction, its quali- and quantitative evaluation and the reverse transcription into cDNA were made according to Zorzan et al. (2016). The full list of primers used for qPCR analysis is reported in Table 1. Candidate genes were *KIT*, the -myc avian myelocytomatosis viral oncogene homolog (*MYC*), the vascular endothelial growth factor A (*VEGFA)*, the Kirsten rat sarcoma viral oncogene homolog *(KRAS)*, the B-cell leukemia/lymphoma 2 *(BCL2)*, and the Telomerase Reverse Transcriptase (*TERT*). The Primer3 software (http://primer3.ut.ee/) was used to design primers; the specificity of each gene assay was evaluated *in silico* by means of the BLAST tool and experimentally by using the Power SYBR Green I (Thermo Fisher Scientific, Waltham, MA, USA) amplification and melting curve analysis.

Quantitative real-time PCR (qPCR) reactions were performed in a LightCycler 480 Instrument (Roche Applied Science, Indianapolis, IN, USA) using 0.83 ng of C2 cells cDNA or 2.5 ng of NI-1 cells cDNA (in a 10 µL final volume) and standard qPCR conditions (95°C

for 10 min; 45 cycles at 95°C for 10 s and at 60°C for 30 s; 40°C for 30 s). Calibration curves were made using three-fold serial dilutions of a cDNA pool, and the values of slope, efficiency (E) and dynamic range obtained with both cell lines are reported in Supplementary Table 1. Only qPCR assays with E comprised between 90% and 110% were considered as acceptable. The obtained qPCR data were analyzed using the LightCycler480 1.5.0 software (Roche Applied Science, Indianapolis, IN, USA) and the second derivative method; the relative quantification (RQ) of target gene mRNA levels was achieved by using the ΔΔCt method (Livak et al., 2001). Four internal control genes (ICGs), i.e. the ATP synthase, H^+ transporting, mitochondrial F1 complex, beta polypeptide (*ATP5β*), the Golgin A1 (*GOLGA1*), the transmembrane BAX inhibitor motif containing 4 (*CGI-119*) and CCZ1 vacuolar protein trafficking and biogenesis associated homolog (*CCZ1*) were selected. These ICGs were amplified in all samples, but only those whose mRNA levels were not statistically modulated by the adopted experimental conditions were used for the RQ of target genes. Moreover, a cDNA pool was used as calibrator. Experiments were performed in triplicate, each one consisting of two biological replicates.

Transcriptional effects of G4 ligands on target genes. Cells were incubated with the vehicle alone (DMSO, 0.1% final concentration) and two sub-cytotoxic doses of G4 ligands, i.e. 1/3 and 2/3 of their half maximal inhibitory concentration (IC_{50}). Specifically, C2 cells were treated with 0.5 µM and 1 µM of AQ1 and 2 µM and 4 µM of AN6 (final concentrations); NI-1 cells were treated with 0.08 µM and 0.16 µM of AQ1 and 0.7 µM and 1.4 µM of AN6 (final concentrations). After 6, 12 and 24 hours of incubation, cell pellets were collected as described above. The expression of the whole set of candidate ICGs was checked within every experimental condition, and the choice of the most suitable ICG for normalization was cell line- and ligand-dependent. A cDNA pool was used as calibrator. Each experiment was performed in triplicate, each one with three biological replicates.

JPET Fast Forward. Published on October 1, 2018 as DOI: 10.1124/jpet.118.248997
This article has not been copyedited and formatted. The final version may differ from this version.

Confirmatory post-translational effects of G4 ligands. The first day of the experiment, C2 and NI-1 cells (5.4 x 10^6 cells/well) were seeded in Petri dishes. C2 cells were treated for 24 hours with AQ1 (1.5 µM), AN6 (4 µM) or DMSO (0.1%) while NI-1 were treated with 0.23 µM of AQ1, 1.4 µM of AN6 or 0.1% of DMSO. After washing with PBS 1X with 0.02% EDTA, cell pellets were resuspended in RIPA buffer (50 mM Tris-HCl pH 7.4, 1% Triton X-100, 0.5% Na-deoxycholate, 0.1% SDS, 150 mM NaCl, 2 mM EDTA, 0.2 mM sodium orthovanadate, 1% protease inhibitor cocktail, Sigma-Aldrich Co., St. Louis, USA), incubated for 30 min on an ice bed and centrifuged for 10 min at high speed. Proteins were separated in 4-12% NuPAGE® Novex® Bis-Tris Gels (Thermo Fisher Scientific, Waltham, MA, USA) by using the XCell SureLock™ Mini-Cell electrophoresis system (Thermo Fisher Scientific, Waltham, MA, USA), and transferred onto nitrocellulose filters through the iBlot™ Dry Blotting System (Thermo Fisher Scientific, Waltham, MA, USA). On each gel, one pre-stained molecular marker (Thermo Scientific PageRuler Plus Prestained Protein Ladder, Thermo Fisher Scientific, Waltham, MA, USA), an unstained molecular marker (MagicMark™ XP Western Protein Standard, Thermo Fisher Scientific, Waltham, MA, USA), and a c-kit positive control (TF1 cells stable transfected with KITD816V, kindly provided by Drs. Patrice Dubreuil and Paulo De Sepulveda, Centre de Recherche en Cancérologie, Marseille, France) were loaded. Membranes were incubated with goat polyclonal antibodies (1:1000) raised against human c-kit (C-14, Santa Cruz Biotechnology, Dallas, Texas, USA) and human glyceraldehyde 3-phosphate dehydrogenase (GAPDH, V-18, Santa Cruz Biotechnology, Dallas, Texas, USA). The secondary antibody consisted in a peroxidase-conjugated anti-goat IgG (Merck Spa, Milano, Italy). The peroxide signal was detected using the Super Signal West Pico Chemiluminescent Substrate Kit (Thermo Fisher Scientific, Waltham, MA, USA). Images were captured by Canon MG 5150 (Canon, Ōta, Tokyo, Japan) and the integrated optimal density of each band was measured with the

JPET Fast Forward. Published on October 1, 2018 as DOI: 10.1124/jpet.118.248997
This article has not been copyedited and formatted. The final version may differ from this version.

program ImageJ (https://imagej.net). Data were normalized with GAPDH values, and the band corresponding to TF1 KITD816V was used as a reference.

Plasmid construct and dual-luciferase reporter assay. Part of the canine *KIT* proximal promoter (-228/-24) was subcloned, at the KpnI/ SacI sites, into the reporter plasmid pGL4.10 expressing the firefly luciferase (Promega, Madison, WI, USA). Two different plasmids (pGL4.10Δkit_A and pGL4.10Δkit_G) were obtained, according to the polymorphism detected in d_kit2 sequence in position -159 (Da Ros et al., 2014). Each plasmid was sequenced to check for the correct insert ligation. MDCK cells (5.0×10^3 cells in 96-well plates) were co-transfected with 80 ng of pGL4.10Δkit_A or pGL4.10Δkit_G and 20 ng of the Renilla control plasmid pGL4.74 (Promega, Madison, WI, USA), using the Fugene HD Transfection reagent (ratio 4:1, Promega, Madison, WI, USA). Twenty-four hours later, the medium was changed and cells incubated with AQ1 or AN6 (8 μM final concentration). After 48 hours, the Dual-Glo luciferase assay kit (Promega, Madison, WI, USA) was used to measure the luciferase activity. The firefly signal derived from the reporter plasmid was normalized to the Renilla luciferase signal.

Statistical analysis. Data statistical analysis was performed by using GraphPad Prism version 5.00 for Windows (GraphPad Software, San Diego, CA, USA). Dose-response curves and IC_{50} values were determined by nonlinear regression analysis, fitting a sigmoid dose-response curve. Data of time-dependent constitutive expression of target genes were expressed as n-fold change of the value obtained at T_6, and analyzed with one-way analysis of variance (ANOVA) followed by Bonferroni's post-test. A two-way ANOVA followed by Bonferroni's post-test was used to analyze data from cells treated with G4 ligands to verify if any difference in transcriptional response was dose- and/or time-dependent. Each RQ value of treated cells was normalized to the average RQ of the respective time-control samples. Immunoblotting data were expressed as a percentage of control integrated density, where

control was represented by normal cells in culture. Variations between DMSO- and G4 ligands exposed cells were statistically evaluated using the Student *t*-test. Transfection data were expressed as a ratio between luciferase firefly/luciferase renilla control activation signal normalized to the control one; this latter was represented by the empty vector or DMSO-treated cells. The observed variations were statistically evaluated using non-parametric one-way ANOVA followed either by the Dunn's post-test (when a comparison between three groups was made) or the non-parametric Student *t*-test (when only two groups were considered). Overall, a P value ≤ 0.05 was considered as statistically significant.

JPET Fast Forward. Published on October 1, 2018 as DOI: 10.1124/jpet.118.248997
This article has not been copyedited and formatted. The final version may differ from this version.

RESULTS

Sequencing of *KIT* proximal promoter in canine C2 and NI-1 cells. Before testing the effects of candidate G4 ligands, we verified if C2 and NI-1 cells possessed the expected d_kit1 and d_kit2 sequences already characterized by Da Ros et al. (2014). In particular, we focused on nucleotide -159, owing to a polymorphism (-159 G>A) that we previously noticed in a cohort of canine MCTs. The d_kit1 and d_kit2 sequences were the following ones: d_kit1, AGGGAGGGCGCCGGGAGGAGGG; d_kit2, AGGAGGGGCGCGGGGAAGGGG. Therefore, considering the nomenclature previously reported by Da Ros and co-authors (2014), it was inferred that C2 and NI-1 cells possess both d_kit1 and d_kit2_A16 sequences.

Interaction of G4 forming sequences with selected ligands. As we previously reported, the conformational features of G-rich domains of human and canine *KIT* promoters only partially overlap. In particular, while a general conservation was found between the kit1 domain of the two species, the conformational features of h_kit2 and d_kit2_A16 significantly diverge. Therefore, we preliminarly explored the interaction of our two G4 ligands with canine sequences. Specifically, we assessed the G4 thermal stabilization induced by our ligands using a fluorescence melting assay, and the ligands binding to G4 using a fluorescence competitive displacement assay in which TO was used as a probe. Both protocols highlighted a binding profile of canine sequences relatively similar to the human one, and confirmed a preferential binding of AQ1 to all the tested G-rich sequences (Table 2). The same behavior was noticed using a double stranded DNA (dsDNA) that did not fold into G4, thus reminding the possible higher rate of off-target effects connected to the use of AQ1.

As a second step we decided to assess if the observed G4 interaction was predictive for an interference with DNA processing enzymes. Thus, we analyzed the replication of template strands containing either the human or the canine kit1 and kit2 sequences. In this experimental system, G4 formation is expected to stop the elongation of a complementary

primer by Taq polymerase (Polymerase Stop assay). Consistently, increasing concentrations of our ligands in the reaction mixture resulted in a progressive reduction of the full length product and in the parallel formation of an arrest product corresponding to the primer elongation up to the G-rich domain. The intensities of corresponding bands were quantified and the % of the truncated form over the total elongated products was plotted as a function of ligand concentration (Fig. 1). The effects elicited by the tested derivatives did not significantly differ between the two species: in particular, as already reported for human sequences and in agreement with the DNA binding profile, AQ1 was the most effective in fully suppress the elongation of all templates. Additionally, in the presence of low ligands concentrations, kit2 represented always the preferential arrest site if compared to kit1. It is worth to point out that these results were obtained using simplified models that take into account only the single strand G-rich sequences whereas, inside the cell, the promoter is essentially present as a double stranded DNA. This represents a challenge for G4 ligands; in fact, to be physiologically effective they must support a dsDNA un-pairing in order to free the G-rich strand and to promote its G4 folding. To verify the ability of our compounds to shift the DNA conformational equilibria from ds to G4 folding, a fluorescence melting study was performed. As target sequences we used both the human and canine G-rich domains previously paired to their complementary C-rich strands. In our system, the G-rich strands were labelled at 3' and 5' with a fluorophore and a quencher, respectively: this allowed monitoring the melting of the double helix whenever associated to the formation of a G4 structure as a remarkable quenching of the fluorescence signal (Rachwal and Fox, 2007, Bhattacharjee et al., 2011, Wang and Wei, 2013). In our experimental conditions (50 mM KCl), the conversion of dsDNA into a G4 structure was evident above 60°C (Fig. 2). A further increase in the temperature is also expected to result in the G4 denaturation (Alberti et al., 2003, Koirala et al., 2013), but in our experimental conditions this event was well

JPET Fast Forward. Published on October 1, 2018 as DOI: 10.1124/jpet.118.248997
This article has not been copyedited and formatted. The final version may differ from this version.

resolved only with the h_kit2 sequence. This means that for the other sequences the thermal stability of the G4 folded form is not significantly higher than the dsDNA.

Next, the same protocol was repeated by including increasing concentrations of our ligands in the reaction mixture (Fig 3). Overall, the presence of the ligands allowed to properly detect both the ds-G4 conversion and the G4 melting, thus highlighting a preferential stabilization of the tetrahelical conformation. The only exception was represented by the d_kit2_A16 sequence, where no G4 melting was actually ever detected.

Cytotoxicity. By using the Alamar Blue cytotoxity test, a sigmoidal dose-response curve was built up for each ligand in canine C2 cell line, and the corresponding IC_{50} value identified. In Fig. 4, dose-response curves for AQ1 (Fig. 4A) and AN6 (Fig. 4B) are reported. The obtained IC_{50} values were 1.27 μM (R^2: 0.9813) and 5.87 μM (R^2: 0.9721) for AQ1 and AN6, respectively.

Results of confirmatory cytotoxicity assays made in the NI-1 cell line (dose-response curves and corresponding IC_{50} values) are reported in Supplementary Fig. 1. Both ligands were proved to be cytotoxic. This MCT cell line was more sensitive if compared with C2 cells, as shown by the lower IC_{50} values we obtained (0.23 μM and 2 μM for AQ1 and AN6, respectively).

Time-dependent constitutive expression of target genes. Target gene mRNA levels are likely to change with time of culture; therefore, we measured in both the canine MCT cell lines the possible time-dependent changes (from 6 and up to 96 hours) in the constitutive expression of *KIT* and other five genes known to contain putative G4 structures in their promoter. Overall, some differences were noticed between the two cell lines. In C2 cell line (Fig. 5), *KIT* and *KRAS* mRNA levels were never affected by the time of culture, while an overall decrease was noticed for *BCL2*, *MYC* and *TERT*. Specifically, *BCL2* mRNA levels were significantly decreased at T_{96} vs T_{24} and T_{48} ($P<0.05$); *MYC* constitutive expression was

significantly decreased at $T_{48,}$ T_{72} and T_{96} vs T_6 (P<0.05); *TERT* showed a higher pattern of expression up to T_{24}; then, it showed a significant decrease at T_{96} vs T_6 and T_{24} (P<0.001); finally, *VEGFA* was the unique gene showing a time-dependent upregulation of its mRNA levels, reaching the level of significance at T_{96} vs T_{24} and T_{48} (P<0.001 and P<0.05, respectively).

In NI-1 cells (Supplementary Fig. 2), *KIT* mRNA levels slightly increased with time (T_6 and T_{24} vs T_{96}; P<0.05) while no time-dependent changes were ever noticed for *BCL2*, *KRAS* and *MYC* mRNA levels. However, *TERT* showed a slight inhibition at T_{72} and T_{96} (P<0.05), while a time-dependent *VEGFA* upregulation, reaching the level of significance at T_{96} vs T_6 (P<0.05), was observed.

Taking these results into consideration as a whole, we decided to measure the transcriptional effects of two sub-cytotoxic concentrations of AQ1 and AN6 (corresponding to 1/3 and 2/3 of their IC_{50}) and at three different time-points (T_6, T_{12} and T_{24} hours post-exposure) in both cell lines.

Transcriptional effects of G4 ligands and confirmatory post-translational investigations. An overall dose-dependent decrease of *KIT* mRNA was observed in C2 cells exposed to AQ1, reaching the level of statistical significance at T_{24} (P<0.05, P<0.01; Fig. 6A). No differences were ever recorded for the other target genes (data not shown) except for *BCL2*, for which an overall and moderate downregulation was noticed. Such a decrease was proved significant at the highest dose at T_{12} (P<0.05: Fig. 6B). As *KIT* was the main target of this study, we made a confirmatory set of similar experiments using a higher AQ1 concentration (1.5 μM). We observed a greater gene downregulation, significant at earlier time-points (T_6 and T_{12}; P<0.05, Fig. 7A). Furthermore, these transcriptional results were also confirmed at the protein level, as shown in Fig. 7B-C. The densitometric analysis showed a significant (P<0.05) two-fold reduction of c-kit protein following the treatment with AQ1.

As regards AN6, we observed an overall and dose-dependent inhibition of *KIT* mRNA levels. This downregulation was always significant ($P<0.01$ at T_6 and T_{24} $P<0.05$ at T_{12}) at the highest ligand concentration (4 μM), and limited to T_{24} ($P<0.05$) in cells exposed to 2 μM AN6 (Fig. 8A). Confirmatory post-transcriptional investigations pointed out a two-fold significant ($P<0.05$) decrease of c-kit protein after 24 hours of exposure with 4 μM AN6 (Figure 8, B-C). The other target genes showed neither time- or dose-dependent significant variations of mRNA levels (data not shown).

Fairly similar confirmatory results were obtained with NI-1 cells. In Supplementary Fig. 3A-B we show *KIT* and *BCL2* mRNA levels measured after the exposure of NI-1 cells, at different time points, to two AQ1 sub-cytotoxic concentrations. A significant downregulation of *KIT* mRNA level was detected at T_6 ($P<0.001$) and T_{12} ($P<0.01$, $P<0.001$; Supplementary Fig. 3A), while a significant *BCL2* downregulation was observed at T_6 and only at the highest AQ1 concentration ($P<0.01$; Supplementary Fig. 3B). No differences were recorded for the other target genes (data not shown). When NI-1 cells were treated with a higher AQ1 concentration, a greater gene downregulation was noticed at the same time-points ($P<0.001$ and $P<0.05$ at T_6 and T_{12}, respectively; Supplementary Fig. 4A). These transcriptional results were also confirmed at the protein level (Supplementary Fig. 4B). The densitometric analysis showed a significant ($P<0.01$) two-fold reduction of c-kit protein following the treatment with AQ1.

The treatment with AN6 led to a significant inhibition of *KIT* expression at higher dose and within the first 12 h of treatment ($P<0.01$ and $P<0.001$ at T_6 and T_{12}, respectively; Supplementary Fig. 5A). Post-transcriptional investigations corroborated transcriptional results, with a significant ($P<0.05$) decrease of c-kit protein after 24 hours of exposure with AN6 treatment (Supplementary Fig. 5B). The other target genes never showed time- or dose-dependent significant variations of their mRNA levels (data not shown).

Dual-luciferase reporter assay. To explore if the effects of AQ1 and AN6 on *KIT* expression were consequent to the ligand binding to *KIT* proximal promoter, a canine non-cancerous cell line (MDCK) was transfected with canine *KIT* proximal promoter sequence cloned upstream of a luciferase reporter gene. Cells transfected with the plasmid containing the canine *KIT* proximal promoter increased more than fifteen-fold ($P<0.001$) the luciferase production when compared with those transfected with the empty pGL4.10 reporter plasmid (Fig. 9). This result was indicative of the presence of transcription binding sites in DNA sequence immediately upstream the transcription starting site (TSS), just where d_kit1 a d_kit2_A16 G4 are located.

Then, to find the suitable sub-cytotoxic concentration of AQ1 and AN6 to be used in gene reporter assays, MDCK cells were exposed for 48 hours to increasing concentrations of each ligand (from 0.05 µM up to 12 µM: Fig. 10A-B). Results proved MDCK are highly resistant to the treatment with the two candidate G4 ligands. Indeed, both AQ1 and AN6 halved the cell viability at 10 µM; specifically, cells exposed to 8 µM AQ1 showed about 70% of viability, while no cytotoxicity was noticed with 8 µM AN6.

Following the transfection of MDCK cells with pGL4.10Δkit_A or pGL4.10Δkit_G plasmid for 24 hours, and the ensuing incubation for 48 hours with both G4 ligands (8 µM final concentration), AQ1 did not modify substantially the luciferase activity (Fig. 10C); however, this latter one was significantly inhibited ($P<0.001$) by AN6 (Fig. 10D). This inhibition was not influenced by the presence of the G>A polymorphism.

JPET Fast Forward. Published on October 1, 2018 as DOI: 10.1124/jpet.118.248997
This article has not been copyedited and formatted. The final version may differ from this version.

DISCUSSION

The presence of G4 structures in genome regions that are essential for cell proliferation got the interest of researchers in their use as potential targets for anticancer agents; as a result, a number of small molecules showing either good G4 interaction and promising cytotoxic activity *in vitro* were considered as candidate anticancer drugs. Overall, the fundamental similarities between canine and human tumours suggest their possible translation from one species to the other. However, this strategy can easily fails when we deal with G4-directed ligands. Indeed, these nucleic acid structures are highly polymorphic, and even negligible sequence mutations can cause large changes in G4 topology and stability. Moreover, this can easily result also in the recruitment of a not conserved transcriptional machinery, where different protein components are involved. To shed light on these events, a comparative and translational approach to cancer research is critically important to ultimately derive benefits for both species and to develop new candidate G4 ligands with realistic drug-like structures, higher selectivity and reduced side effects. Here, we considered that the proximal promoter of human and canine genes presents a relevant degree of sequence homology that, however, does not exclude some partial structural rearrangements. Additionally, mutations located within promoter G-rich domains might be responsible of a partial rearrangement of the associated G4 structures. Ultimately, this might affect their recognition by small G4 ligands and, consequently, it can lead to distinct molecular events (Siddiqui-Jain et al., 2002; Patel et al., 2007; Tian et al., 2010). Nevertheless, this was not the case for human and canine *KIT*; in fact, the inter-species comparison of binding properties of the selected G4 ligands to the canine and human sequences showed only minor variations.

In both species, AQ1 was proved as a stronger binder in comparison to AN6, recognizing both G4 and dsDNA. As already mentioned, the interaction with the double helix was extremely reduced with AN6; hence, we might assume this latter as a more selective G4

JPET Fast Forward. Published on October 1, 2018 as DOI: 10.1124/jpet.118.248997
This article has not been copyedited and formatted. The final version may differ from this version.

binder. Despite this difference in DNA recognition, the AN6-kit2 complex appears to be an interference element for DNA processing enzyme as good as the AQ1-kit2. Thus, we could postulate that treatment of canine or human cancer cells lines with AQ1 or AN6 would cause similar effects on oncogene expression. However, this was not the case.

When using AQ1, a significant downregulation of *KIT* mRNA was noticed after 24 hours of exposure to two sub-cytotoxic concentrations (0.5 µM and 1 µM); furthermore, a time-independent decrease of *KIT* gene expression was observed at a concentration close to the corresponding IC_{50} value (1.5 µM). This gene downregulation was confirmed at the protein level when C2 cells were exposed to the same AQ1 concentration (1.5 µM). In confirmatory studies made on a second canine MCT cell line (NI-1), the cell proliferation was substantially inhibited at lower AQ1 concentrations; moreover, and fairly similar to C2 cell line, the exposure to AQ1 sub-cytotoxic concentrations resulted in a significant downregulation of *KIT* mRNA levels and c-kit protein. Nevertheless, such an inhibition in canine models is less pronounced if compared with the one we obtained in the human mast cell leukemia cell line HMC1.2 (i.e., two-fold vs five-fold decrease in dog vs human cell line, respectively, Zorzan et al., 2016). Concerning the selectivity of AQ1 transcriptional effects, we screened other oncogenes containing putative G4 structures in their promoter (*MYC, VEGFA, KRAS, BCL2*, and *TERT*). Overall, only *BCL2* showed a trend to mRNA downregulation in both canine cell lines. This result was not unexpected; in fact, AQ1 caused a marked inhibition of *BCL2* mRNA levels in human cell lines, too (Zorzan et al., 2016); moreover, some anthraquinone derivatives have been shown to induce apoptosis *in vitro*, and such a phenomenon usually implies a decrease of *BCL2* mRNA/protein (Dong et al., 2017; Hasan et al., 2011; Huang et al., 2007; Huang et al., 2014). This promising picture did not overlap the results we obtained with the luciferase reporter assay, showing an extremely reduced capability of AQ1 to decrease the luciferase production even at the highest tested

concentrations. Considering the results we obtained as a whole, it is conceivable to hypothesize that the mild inhibition observed in canine *KIT* mRNA and protein after the exposure to AQ1 might not univocally derive from the interaction between the ligand and the G4 in the promoter; rather, it might represent the consequence of other molecular mechanisms related to the cellular response to anticancer drugs like, for example, TKIs and doxorubicin (Milovancev et al., 2016; Rossi et al., 2013; van de Ven et al., 2011; Yamada et al., 2011).

In line with the lower DNA binding affinity and with previous data obtained in human cell lines, AN6 was less cytotoxic than AQ1 in C2 and NI-1 cells. Despite this, it significantly decreased *KIT* mRNA levels in both cell lines; additionally, this transcriptional downregulation was confirmed at the protein level. Interestingly, the gene reporter assay showed an inhibition of luciferase activity following the exposure of MDCK cells to AN6. Taken as a whole, these results would confirm the activity of AN6 on canine *KIT* proximal promoter. Nevertheless, such a behavior was quite unexpected. Indeed, in human cell lines exposed to AN6 neither a *KIT* transcriptional inhibition nor a reduction of the coded c-kit protein were ever observed (Zorzan et al., 2016). Therefore, despite the apparent binding affinity for canine G4 domains was AQ1>AN6, the anthracene derivative was proved as a better *KIT* transcriptional down-regulator in canine cell lines. Worth mentioning, an opposite behavior was previously observed in human cell lines. To rationalize this picture, it is worth to underline that: 1) conformational features of canine and human promoter sequences are perfectly overlapping for kit1 but slightly different for kit2; 2) in terms of conformational rearrangements, kit2 is more sensitive to the presence of the ligands and this favors the impairment of DNA processing.

Merging all these data we can try to explain the different chemico-biological behavior we noticed in human and canine cells following the exposure to G4 candidate ligands. If we remind that the main difference between human and canine promoter rests in a preferential

shift of the structural equilibrium towards the double stranded form for d_kit2_A16 in contrast to the G4 as in h_ kit2 and that AQ1 is poorly able to discriminate between these two different nucleic acid structural arrangements, it is tempting to attribute the persistence of luciferase production in transfected cells treated with AQ1 to its inability to convert the paired d_kit2_A16 into a G4. This explanation would further reinforce the importance of G4 domains in *KIT* proximal promoter as regulatory elements. Nevertheless, we cannot forget that the observed differences in the biological effects of the two tested compounds might reflect species-differences in susceptibility (human cells answer otherwise to AN6) and/or the possible involvement of other signaling pathways (*BCL2* and apoptosis). It derives that further studies are clearly needed to deepen the molecular mechanisms resulting from the interaction of these ligands with canine *KIT* G4 structures. For example, chromatin immunoprecipitation might demonstrate whether AN6 (but also AQ1) really binds to d_kit1 and d_kit2 impeding the binding with Sp1 site. Additionally, it is known that approximately 30–40% of human gene promoters contain a putative G4 motif, but no information is currently available about the canine genome. Therefore, we should implement the molecular characterization of genes containing potential G4 structures and found overexpressed in MCT cell lines (i.e., other oncogenes such as *TERT* or *PDGFA*), to ascertain which cellular targets are primarily responsible for the inhibition of tumor cell growth by the G4 ligands here studied. In this scenario, next generation sequencing technologies (e.g., RNA-Seq) might help to unveil specific off-targets of AQ1 and AN6 in canine MCT and non-cancer cells, as *KIT* seems not to be the only one. Another strategy is represented by the development of highly selective G4 ligands, thus avoiding an overall inhibition of gene transcription, potentially resulting in non-specific toxicity.

In conclusion, to the authors' knowledge this is the first *in vitro* study showing how two candidate G4 ligands (AQ1 and AN6), formerly screened in human cells, downregulate *KIT*

expression in canine *KIT*-dependent MCT cell lines, and the anthracene derivative AN6 would represent (mostly) a promising candidate to decrease *KIT* expression in canine *KIT*-dependent tumors such as MCTs.

ACKNOWLEDGMENTS

Authors would thanks Dr. Patrice Dubreuil as well as Prof. Peter Valent and Drs. Emir Hadzijusufovic and Michael Willmann for the obtainment of C2 and NI-1 cell lines, respectively.

The authors gratefully acknowledge undergraduate students Giulia Marostica and Valentina Michielon for their help during cell culturing and fine tuning of qPCR and immunoblotting assays, respectively.

AUTHORSHIP CONTRIBUTIONS

Partecipated in research design: Giantin, Palumbo, Sissi, Dacasto.

Conducted experiments: Zorzan, Shahidian, Da Ros, Guerra.

Performed data analysis: Zorzan, Da Ros.

Wrote or contribute to the writing of the manuscript: Zorzan, Da Ros, Giantin, Sissi, Dacasto.

REFERENCES

Alberti P, and Mergny JL (2003) DNA duplex-quadruplex exchange as the basis for a nanomolecular machine. *Proc Nat Acad Sci USA* **100**: 1569-1573.

Aresu L, Giantin M, Morello E, Vascellari M, Castagnaro M, Lopparelli R, Zancanella V, Granato A, Garbisa S, Aricò A, Bradaschia A, Mutinelli F, and Dacasto M (2011) Matrix metalloproteinases and their inhibitors in canine mammary tumors. *BMC Vet Res* **7**: 33-43.

Balasubramanian S, Hurley LH, and Neidle S (2011) Targeting G-quadruplexes in gene promoters: a novel anticancer strategy? *Nat Rev* **10**: 261-675.

Beaume N, Pathak R, Yadav VK, Kota S, Misra HS, Gautam HK, and Chowdhury S (2013) Genome-wide study predicts promoter-G4 DNA motifs regulate selective functions in bacteria: radioresistance of *D. radiodurans* involves G4 DNA-mediated regulation. *Nucleic Acids Res* **41**: 76–89.

Bejugam M, Sewitz S, Shirude PS, Rodriguez R, Shahid R, and Balasubramanian S (2007) Trisubstituted isoalloxazines as a new class of G-quadruplex binding ligands: small molecule regulation of c-kit oncogene expression. *J Am Chem Soc* **129**: 12926-12927.

Bhattacharjee AJ, Ahluwalia K, Taylor S, Jin O, Nicoludis JM, Buscaglia R, Brad Chaires J, Kornfilt DJ, Marquardt DG, and Yatsunyk LA (2011) Induction of G-quadruplex DNA structure by Zn(II) 5,10,15,20-tetrakis(N-methyl-4-pyridyl)porphyrin. *Biochimie* **93**: 1297-1309.

Bidzinska J, Cimino-Reale G, Zaffaroni N, and Folini M (2013) G-quadruplex structures in the human genome as novel therapeutic targets. *Molecules* **18**:12368-12395.

Bonkobara M (2015) Dysregulation of tyrosine kinases and use of imatinib in small animal practice. *Vet J* **205**:180-188.

Da Ros S, Zorzan E, Giantin M, Shahidian LZ, Palumbo M, Dacasto M, and Sissi C (2014) Sequencing and G-quadruplex folding of the canine proto-oncogene KIT promoter region: might dog be used as a model for human disease? *Plos One* **9**: e103876.

Dash J, Shirude PS, Hsu SD, and Balasubramanian S (2008) Diarylethynyl amides that recognize the parallel conformation of genomic promoter DNA G-quadruplexes. *J Am Chem Soc* **130**: 15950–15956.

Dong X, Fu J, Yin X, Qu C, Yang C, He H, and Ni J (2017) Induction of apoptosis in HepaRG cell line by aloe-emodin through generation of reactive oxygen species and the mitochondrial pathway. *Cell Physiol Biochem* **42**: 685-696.

Du Z, Kong P, Gao Y, and Li N (2007) Enrichment of G4 DNA motif in transcriptional regulatory region of chicken genome. *Biochem Biophys Res Commun* **354**: 1067-1070.

Dubreuil P, Letard S, Ciufolini M, Gros L, Humbert M, Castéran N, Borge L, Hajem B, Lermet A, Sippl W, Voisset E, Arock M, Auclair C, Leventhal PS, Mansfield CD, Moussy A, and Hermine O (2009) Masitinib (AB1010), a potent and selective tyrosine kinase inhibitor targeting KIT. *PLoS One* **4**: e7258.

Fernando H, Reszka AP, Huppert J, Ladame S, Rankin S, Venkitaraman AR, Neidle S, and Balasubramanian S (2006) A conserved quadruplex motif located in a transcription activation site of the human c-kit oncogene. *Biochemistry* **45**: 7854-7860.

Gardner HL, Fenger JM, and London CA (2016) Dogs as a model for cancer. *Annu Rev Anim Biosci* **4**: 199-222.

Giantin M, Baratto C, Marconato L, Vascellari M, Mutinelli F, Dacasto M, and Granato A (2016) Transcriptomic analysis identified up-regulation of a solute carrier transporter and UDP glucuronosyltransferases in dogs with aggressive cutaneous mast cell tumours. *Vet J*. **212**: 36-43.

Giantin M, Granato A, Baratto C, Marconato L, Vascellari M, Morello EM, Vercelli A, Mutinelli F, and Dacasto M (2014) Global gene expression analysis of canine cutaneous mast cell tumor: could molecular profiling be useful for subtype classification and prognostication? *PLoS One* **9**: e95481.

Giantin M, Aresu L, Benali S, Aricò A, Morello EM, Martano M, Vascellari M, Castagnaro M, Lopparelli RM, Zancanella V, Granato A, Mutinelli F, and Dacasto M (2012) Expression of matrix metalloproteinases, tissue inhibitors of metalloproteinases and vascular endothelial growth factor in canine mast cell tumours. *J Comp Pathol* **147**: 419-429.

Gil da Costa RM (2016) C-kit as a prognostic and therapeutic marker in canine cutaneous mast cell tumours: from laboratory to clinic. *Vet J* **205**: 5-10.

Halsey CHC, Gustafson DL, Rose BJ, Wolf-Ringwall A, Burnett RC, Duval DL, Avery AC, and Thamm DH (2014) Development of an in vitro model of acquired resistance to toceranib phosphate (Palladia®) in canine mast cell tumor. *BMC Vet Res* **10**:105-117.

Hadzijusufovic E, Peter P, Herrmann H, Rülicke T, Cerny-Reiterer S, Schuch K, Kenner L, Thaiwong T, Yuzbasiyan-Gurkan V, Pickl WF, Willman M, and Valent P (2012) NI-1: a novel canine mastocytoma model for studying drug resistance and IgER-dependent mast cell activation. *Allergy* **67**: 858-868.

Hasan TN, B LG, Shafi G, Al-Hazzani AA, and Alshatwi AA (2011) Anti-proliferative effects of organic extracts from root bark of *Juglans regia* L. (RBJR) on MDA-MB-231 human breast cancer cells: role of Bcla-2/Bax, caspases and Tp53. *Asian Pac J Cancer Prev* **12**: 525-30.

Huang L, Zhang T, Li S, Duan J, Ye F, Li H, She Z, Gai G, and Yang X (2014) Anthraquinone G503 induces apoptosis in gastric cancer cells through the mitochondrial pathway. *Plos One* **9**: e108286.

Huang Q, Lu G, Shen H, Chung MCM, and Ong CN (2007) Anti-cancer properties of anthraquinones from rhubarb. *Med Res Rev* **27**: 609-630.

Huppert JL, and Balasubramanian S (2007) G-quadruplexes in promoters throughout the human genome. *Nucleic Acids Res* **35**: 406–413.

Kang SG, and Henderson E (2002) Identification of non-telomeric G4-DNA binding proteins in human, E. coli, yeast, and Arabidopsis. *Mol Cells* **14**: 404–410.

Koirala D, Ghimire C, Bohrer C, Sannohe Y, Sugiyama H, and Mao H (2013) Long-loop G-quadruplexes are misfolded population minorities with fast transition kinetics in human telomeric sequences. *J Am Chem Soc* **135**: 2235-2241.

Kota S, Dhamodharan V, Pradeepkumar PI, and Misra HS (2015) G-quadruplex forming structural motifs in the genome of Deinococcus radiodurans and their regulatory roles in promoter functions. *Appl Microbiol Biotechnol* **99**: 9761–9769,

Lipps HJ, and Rhodes D (2009) G-quadruplex structures: in vivo evidence and function. *Trends Cell Biol* **19**: 414-422.

Livak KJ, and Schmittgen TD (2001) Analysis of relative gene expression data using real time quantitative PCR and the 2(-Delta Delta C(T)) Method. *Methods* **25**: 402-408.

London CA, Malpas PB, Wood-Follis SL, Boucher JF, Rusk AW, Rosenberg MP, Henry CJ, Mitchener KL, Klein MK, Hintermeister JG, Bergman PJ, Couto GC, Mauldin GN, and Michels GM (2009) Multi-center, placebo-controlled, double-blind, randomized study of oral toceranib phosphate (SU11654), a receptor tyrosine kinase inhibitor, for the treatment of dogs with recurrent (either local or distant) mast cell tumor following surgical excision. *Clin Cancer Res* **15**: 3856-3865.

Maizels N, and Gray LT (2013) The G4 genome. *PLoS Genet* **9**: e1003468.

McLuckie KI, Waller ZA, Sanders DA, Alves D, Rodriguez R, Dash J, McKenzie GJ, Venkitaraman AR, and Balasubramanian S (2011) G-quadruplex-binding

benzo[a]phenoxazines down-regulate c-KIT expression in human gastric carcinoma cells. *J Am Chem Soc* **133**: 2658-2663.

Milovancev M, Helfand SC, Marley K, Goodall CP, Löhr CV, and Bracha S (2016) Antiproliferative effects of masitinib and imatinib against canine oral fibrosarcoma in vitro. *BMC Vet Res* **12**: 85-98.

Patel DJ, Phan AT, and Kuryavyi V (2007) Human telomere, oncogenic promoter and 5'-UTR G-quadruplexes: diverse higher order DNA and RNA targets for cancer therapeutics. *Nucleic Acids Res* **35**: 7429-7455.

Perrone R, Lavezzo E, Riello E, Manganelli R, Palù G, Toppo S, Provvedi R, and Richter SN (2017) Mapping and characterization of G-quadruplexes in Mycobacterium tuberculosis gene promoter regions. *Sci Rep* **7**: 5743-5754.

Rachwal PA, and Fox KR (2007) Quadruplex melting. *Methods* **43**: 291-301.

Raiber E, Kranaster R, Lam E, Nikan M, and Balasubramanian S (2012) A non-canonical DNA structure is a binding motif for the transcription factor SP1 in vitro. *Nucleic Acids Res* **40**: 1499–1508.

Rankin S, Reszka AP, Huppert J, Zloh M, Parkinson GN, Todd AK, Ladame S, Balasubramanina S, and Neidle S (2005) Putative DNA quadruplex formation within the human c-kit oncogene. *J Am Chem Soc* **127**: 10584-10589.

Rawal P, Kummarasetti VBR, Ravindran J, Kumar N, Halder K, Sharma R, Mukerji M, Das SK, and Chowdhury S (2006) Genome-wide prediction of G4 DNA as regulatory motifs: role of *Escherichia coli* global regulation. *Genome Res* **16**: 644-655.

Rhodes D, and Lipps H J (2015) G-quadruplexes and their regulatory roles in biology. *Nucleic Acids Res* **43**: 8627–8637.

Rossi G, Bertani C, Mari S, Marini C, Renzoni G, Ogilvie G, and Magi GE (2013) Ex vivo evaluation of imatinib mesylate for induction of cell death on canine neoplastic mast cells with mutations in c-Kit exon 11 via apoptosis. *Vet Res Commun* **37**: 101-108.

Siddiqui-Jain A, Grand CL, Bearss DJ, and Hurley LH (2002) Direct evidence for a G-quadruplex in a promoter region and its targeting with a small molecule to repress *c-MYC* transcription. *P Natl Acad Sci USA* **99**: 11593-11598.

Teng FY, Hou XM, Fan SH, Rety S, Dou SX, and Xi XG (2017) *Escherichia coli* DNA polymerase I can disrupt G-quadruplex structures during DNA replication. *FEBS J* **284**: 4051-4065.

Tian M, Zhang X, Li Y, Ju Y, Xiang J, Zhao C, and Tang Y (2010) Inducement of G-quadruplex DNA forming and down-regulation of oncogene c-myc by bile acid-amino acid conjugate-BAA. *Nucleosides Nucleotides Nucleic Acids* **29**: 190-199.

Van de Ven R, Verbrugge SE, Reurs AW, Bontkes HJ, Hooijberg E, Jansen G, Scheper RJ, Scheffer GL, and de Gruijl TD (2011) High susceptibility of c-KIT^{+}CD34^{+} precursors to prolonged doxorubicin exposure interferes with Langerhans cell differentiation in a human cell line model. *Cancer Immunol Immunother* **60**: 943-951.

Verma A, Halder K, Halder R, Yadav VK, Rawal P, Thakur RK, Mohd F, Sharma A, and Chowdhury S (2008) Genome-wide computational and expression analyses reveal G-quadruplex DNA motifs as conserved *cis*-regulatory elements in human and related species. *J Med Chem* **51**: 5641-5649.

Yamada O, Kobayashi M, Sugisaki O, Ishii N, Ito K, Kuroki S, Sasaki Y, Isotani M, Ono K, Washizu T, and Bonkobara M (2011) Imatinib elicited a favourable response in a dog with a mast cell tumor carrying a c-kit c.1523A>T mutation via suppression of constitutive KIT activation. *Vet Immunol Immunopathol* **142**: 101-106.

Zhao Y, Du Z, and Li N (2007) Extensive selection for the enrichment of G4 DNA motifs in transcriptional regulatory regions of warm blooded animals. *FEBS Lett* **581**: 1951-1956.

Zorzan E, Da Ros S, Musetti C, Shahidian LZ, Coelho NFR, Bonsembiante F, Létard S, Gelain ME, Palumbo M, Dubreuil P, Giantin M, Sissi C, and Dacasto M (2016) Screening of candidate G-quadruplex ligands for the human c-KIT promotorial region and their effects in multiple in-vitro models. *Oncotarget* **7**: 21658-21675.

Wang L, and Wei C (2013) Spectroscopic and biological studies of phenanthroline compounds: selective recognition of gene-promoter G-quadruplex DNAs preferred over duplex DNA. *Chem Biodivers* **10**: 1154-1164.

FOOTNOTES

This work was supported by grants from the University of Padua (CPDA114388, CPDA147272) to M. Dacasto and C. Sissi. E. Zorzan and S. Da Ros were recipient of Ph.D. fellowships and one year post-doc grant fellowships from the University of Padua.

Preliminary results were presented at the 5th International Meeting on Quadruplex Nucleic Acids (Bordeaux, France, May 26th - 28th 2015) as well as at the Annual Congress of the European Society of Veterinary Oncology (Krakow, Poland, May 28th-30th, 2015) and were published in the Congress Proceedings.

[1] Current affiliation: Institute of Functional Epigenetics, Helmholtz Zentrum München, Neuherberg, Germany.

JPET Fast Forward. Published on October 1, 2018 as DOI: 10.1124/jpet.118.248997
This article has not been copyedited and formatted. The final version may differ from this version.

FIGURE LEGENDS

Fig. 1: **Quantification of the arrest product detected by polymerase stop assay**. Experiments were performed with increasing concentration of AQ1 (A) or AN6 (B) and using template strands containing the human or canine kit1 or kit2 sequences. Errors were ± 10%.

Fig. 2. Denaturation profiles of double stranded form of human and canine *KIT* sequences. Data were acquired in presence of 50 mM KCl.

Fig. 3. **Denaturation profiles of the double stranded form of human and canine *KIT* sequences.** Data were acquired in presence of 50 mM KCl and increasing concentrations of AQ1 or AN6. (A) h_kit1 and AQ1; (B) h_kit1 and AN6; (C) d_kit1 and AQ1; (D) d_kit1 and AN6; (E) h_kit2 and AQ1; (F) h_kit2 and AN6; ((G) d_kit2_A16 and AQ1; (H) d_kit2_A16 and AN6.

Fig. 4. Cytotoxicity (dose-response curves) of AQ1 and AN6 in the canine cancer C2 MCT cell line. C2 cells were exposed to AQ1 (A) and AN6 (B) and their cytotoxicity measured using the Alamar blue assay. Cytotoxicity was calculated as [100-(T/control mean*100)]. Data are expressed as mean values ± standard deviation (S.D.) of three independent experiments (each concentration performed in sestuplicate) performed in different culture passages.

Fig. 5. **Effects of culturing time (6, 24, 48, 72, 96 hours) on the expression of genes containing putative G4 structures in their promoter in the canine C2 MCT cell line.** Total RNA was isolated from C2 cells and *KIT, BCL2, VEGFA, KRAS, MYC* and *TERT*

mRNA levels were measured using qPCR. Data (arithmetic means± S.D.) are expressed as n-fold change (a.u.) normalized to the RQ mean value of cells stopped at T_6, to whom an arbitrary value of 100 was assigned. Experiments were performed in triplicate and, for each experiment, three biological replicates were included. The one-way ANOVA was used to measure statistical differences between different times culture. *: $P<0.05$; ***: $P<0.001$.

Fig. 6. Effect of AQ1 (0.5 µM and 1 µM) on *KIT* (A) and *BCL2* (B) mRNA levels in the canine C2 MCT cell line. Gene expression profiles were measured by using qPCR, and data (arithmetic means ± S.D.) are expressed as n-fold change (a.u.) normalized to the RQ value of corresponding control cells (T_6, T_{12}, T_{24}) to whom an arbitrary value of 1 was assigned. Experiments were performed in triplicate and, for each experiment, three biological replicates were included. Two-way ANOVA and Bonferroni post-test were used to check for statistical differences between doses and time of treatment. *: $P<0.05$; **: $P<0.01$.

Fig. 7. Effect of AQ1 (1.5 µM) on *KIT* gene expression (A) and c-kit protein (B-C) in the canine C2 MCT cell line. (A) *KIT* mRNA levels were measured by qPCR, and data (arithmetic means ± S.D.) are expressed as n-fold change (a.u.) normalized to the RQ of control cells at each time (T_6, T_{12}, T_{24}), to whom an arbitrary value of 1 was assigned. Experiments were performed in triplicate and, for each experiment, three biological replicates were included. Two-way ANOVA and Bonferroni post-test were used to find out statistical differences between doses and time of treatment. (B) The effect of AQ1 on c-kit protein amount was measured by using immunoblotting after 24 hours of incubation, and data are expressed as n-fold change (a.u.) with respect to the untreated cells densitometry. Experiments were performed in triplicate and, for each experiment, three biological replicates were included. The Student *t*-test was used to check for statistical differences between cells

treated with AQ1 and those treated with the vehicle only (DMSO). *,**: $P<0.05$; $P<0.01$. In panel C, a representative immunoblot image is reported. Legend: 1, ladder; 2-3, control cells; 4-5, DMSO (vehicle); 6-7, cells exposed to AQ1 (24 hours); 8, TF1 control cells; 9, ladder.

Fig. 8. Effect of AN6 (2 µM and 4 µM) on *KIT* mRNA (A) and c-kit protein (B-C) in the canine C2 MCT cell line. (A) *KIT* mRNA levels were measured by qPCR, and data (arithmetic means ± S.D.) are expressed as n-fold change (a.u.) normalized to the RQ of control cells at each time (T_6, T_{12}, T_{24}), to whom an arbitrary value of 1 was assigned. Experiments were performed in triplicate and, for each experiment, three biological replicates were included. Two-way ANOVA and Bonferroni post-test were used to find out statistical differences between doses and time of treatment. (B) The effect of AN6 on c-kit protein amount was measured by immunoblotting after 24 hours of incubation, and data are expressed as n-fold change (a.u.) with respect to the untreated cells densitometry. Experiments were performed in triplicate and, for each experiment, three biological replicates were included. The Student t-test was used to check for statistical differences between cells treated with AN6 and those treated with the vehicle only (DMSO). *,**: $P<0.05$; $P<0.01$. In panel C, a representative immunoblot image is shown. Legend: 1-2, control cells; 3-4, DMSO (vehicle); 5-6, cells exposed to AN6 (24 hours); 7, TF1 control cells.

Fig. 9. Presence of transcription binding sites in canine *KIT* proximal promoter. *KIT* proximal promoter was cloned into a pGL4.10 luciferase vector and transfected into MDCK cells. The transcriptional activity was assessed by using dual luciferase assays. Data are expressed as the ratio firefly/renilla (a.u.) normalized against cells transfected with empty pGL4.10 vector. Data (means ± SD) of three independent experiments, each one performed in

JPET Fast Forward. Published on October 1, 2018 as DOI: 10.1124/jpet.118.248997
This article has not been copyedited and formatted. The final version may differ from this version.

sestuplicate, are expressed as fold activation (a.u.) to whom an arbitrary value of 1 was assigned. ***: $P<0.001$.

Fig. 10. Effect of the exposure to increasing concentrations of AQ1 (A) and AN6 (B) on canine MDCK (non-cancer) cell line proliferation and dual-luciferase reporter assays (panels C-D). Data referring to the effect of increasing concentrations of AQ1 (A) and AN6 (B) upon MDCK cell proliferation after 48 hours of incubation. Data are expressed as the percentage of survival cells (T/mean controls*100), and they represent means ± S.D. of three independent experiments, each one performed in sestuplicate. As regards the luciferase reporter assays of MDCK cells exposed to either AQ1 (C) or AN6 (D), data are expressed as the ratio firefly/renilla (a.u.) normalized against cells treated with the vehicle (DMSO). Experiments were performed in triplicate and, for each experiment, six biological replicates were included. A non-parametric Student *t*-test was used to check for statistical differences between DMSO and ligand-treated cells. ***: $P<0.001$

JPET Fast Forward. Published on October 1, 2018 as DOI: 10.1124/jpet.118.248997
This article has not been copyedited and formatted. The final version may differ from this version.

TABLES

Table 1. Primers and probes used for qPCR analyses.

Gene	Sequence	Source	UPL probe
ATP5β	F: TCTGAAGGAGACCATCAAAGG	Giantin et al., 2014	#120
	R: AGAAGGCCTGTTCTGGAAGAT		
BCL2	F: ACAACGGAGGCTGGGAATG	designed *ex novo*	#110
	R: CCTTCAGAGACAGCCAGGAGAA		
CCZ1	F: TGAAGCACTGCATTTAATTGTTTAT	Giantin et al., 2016	#148
	R: CTTCGGCAAAAATCCAATGT		
CGI-119	F: TCTACAATCTAAGAGAGATTTCAGCAA	Aresu et al., 2011	#15
	R: TTCCTGACAAGCACAAAATCC		
GOLGA1	F: GGTGGCTCAGGAAGTTCAGA	Aresu et al., 2011	#149
	R: TATACGGCTGCTCTCCTGGT		
KIT	F: CCTTGGAAGTAGTAGATAAAGGATTCA	designed *ex novo*	#60
	R: CAGATCCACATTCTGTCCATCA		
KRAS	F: TGTGGTAGTTGGAGCTGGTG	designed *ex novo*	#62
	R: TCCCTCATTGCACTGTACTCCT		
MYC	F: GCTGCACGAGGAGACACC	designed *ex novo*	#77
	R: TCAATTTCTTCTTCGTCCTCTTG		
TERT	F: TGACGTGGAAGATGAAGGTG	designed *ex novo*	#128
	R: CTCTCTCCGACGGTGTTC		
VEGFA	F: CGTGCCCACTGAGGAGTT	Giantin et al., 2012	#9
	R: GCCTTGATGAGGTTTGATCC		

ATP5β, ATP synthase, H^+ transporting, mitochondrial F1 complex, beta polypeptide; *BCL2*, B-cell leukemia/lymphoma 2; *CCZ1*, vacuolar protein trafficking and biogenesis associated homolog; *CGI-119*, transmembrane BAX inhibitor motif containing 4; *GOLGA1*, Golgin A1; *KIT*, v-kit Hardy-Zuckerman 4 feline sarcoma viral oncogene homolog; *KRAS*, Kirsten rat

sarcoma viral oncogene homolog; *MYC*, v-myc avian myelocytomatosis viral oncogene homolog; *TERT*, telomerase reverse transcriptase; *VEGFA*, vascular endothelial growth factor A; UPL, Universal Probe Library.

JPET Fast Forward. Published on October 1, 2018 as DOI: 10.1124/jpet.118.248997
This article has not been copyedited and formatted. The final version may differ from this version.

Table 2. Thermal stabilization of G-rich sequences of human and canine *KIT* promoter induced by 1 µM of candidate ligands (ΔTm °C) as well as of ligand concentrations (µM) causing a 50% displacement of TO (EC_{50}). dsDNA refers to a random dsDNA.

		h_kit1	**d_kit1**	**h_kit2**	**d_kit2_A16**	**dsDNA**
AQ1	ΔTm (°C)	13.1	18.7	15.3	n.d.	4.6
	EC_{50} (µM)	0.32 ± 0.05	0.64 ± 0.04	0.35 ± 0.05	0.14 ± 0.01	3.66 ± 0.08
AN6	ΔTm (°C)	5.2	1.4	8.0	3.9	0.8
	EC_{50} (µM)	4.11 ± 0.70	5.71 ± 0.46	3.63 ± 1.00	5.11 ± 0.29	11.42 ± 0.28

dsDNA, random double strand DNA; EC_{50}, half maximal effective concentration; h_kit1: human kit1 G4 forming sequence; d_kit1, canine kit1 G4 forming sequence; h_kit2, human kit2 G4 forming sequence; d_kit2_A16: canine kit2 G4 forming sequence with the -159 G>A single nucleotide polymorphism; n.d., the thermal denaturation profiles did not provide a detectable melting transition; TO, thiazole orange.

JPET Fast Forward. Published on October 1, 2018 as DOI: 10.1124/jpet.118.248997
This article has not been copyedited and formatted. The final version may differ from this version.

FIGURES

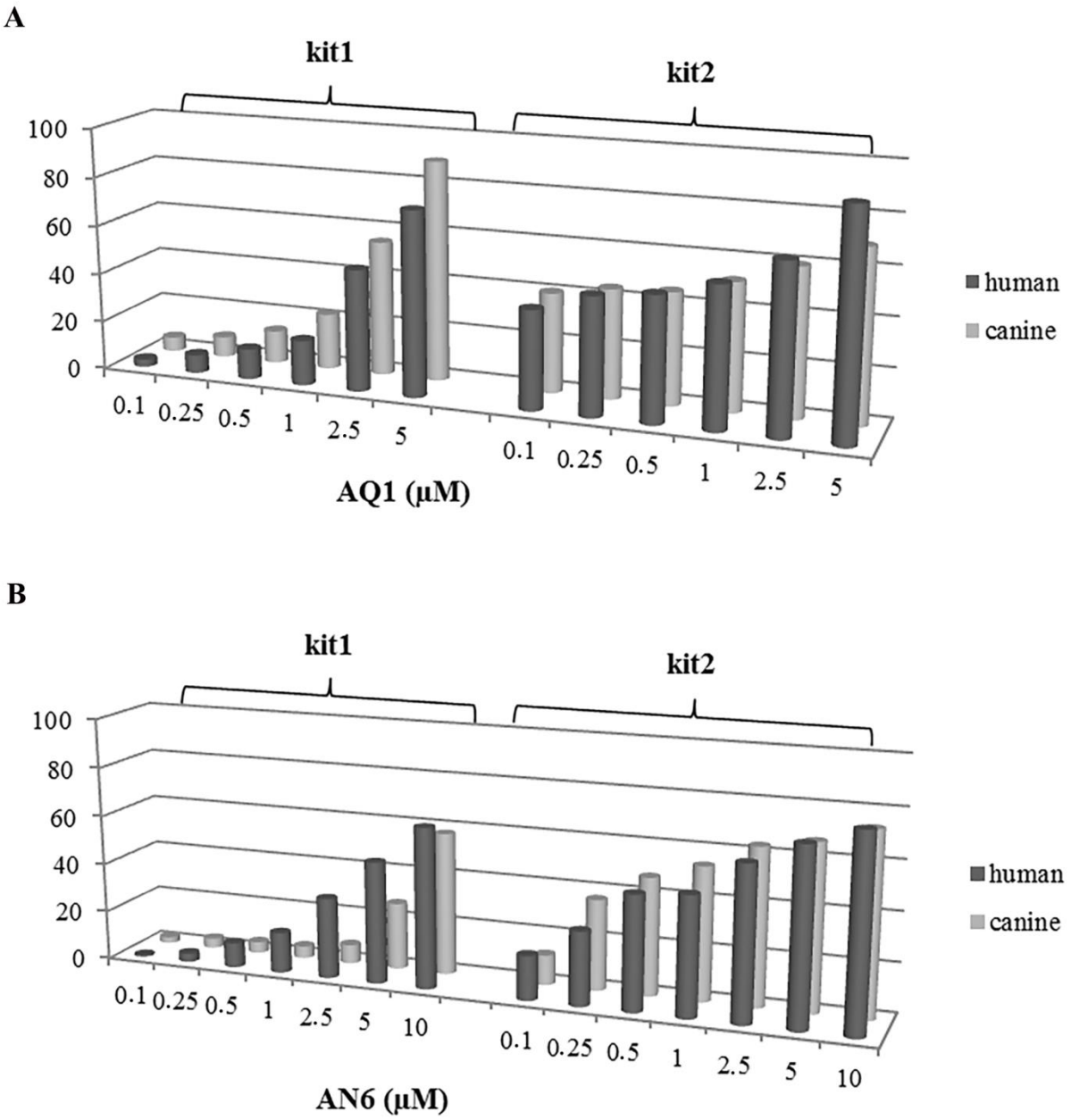

Figure 1

JPET Fast Forward. Published on October 1, 2018 as DOI: 10.1124/jpet.118.248997
This article has not been copyedited and formatted. The final version may differ from this version.

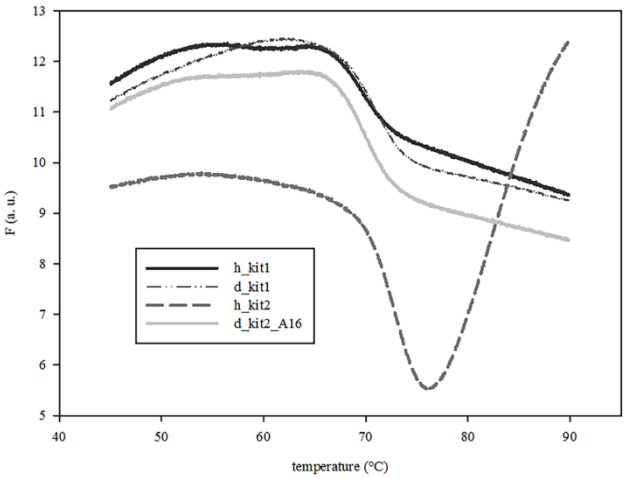

Figure 2

JPET Fast Forward. Published on October 1, 2018 as DOI: 10.1124/jpet.118.248997
This article has not been copyedited and formatted. The final version may differ from this version.

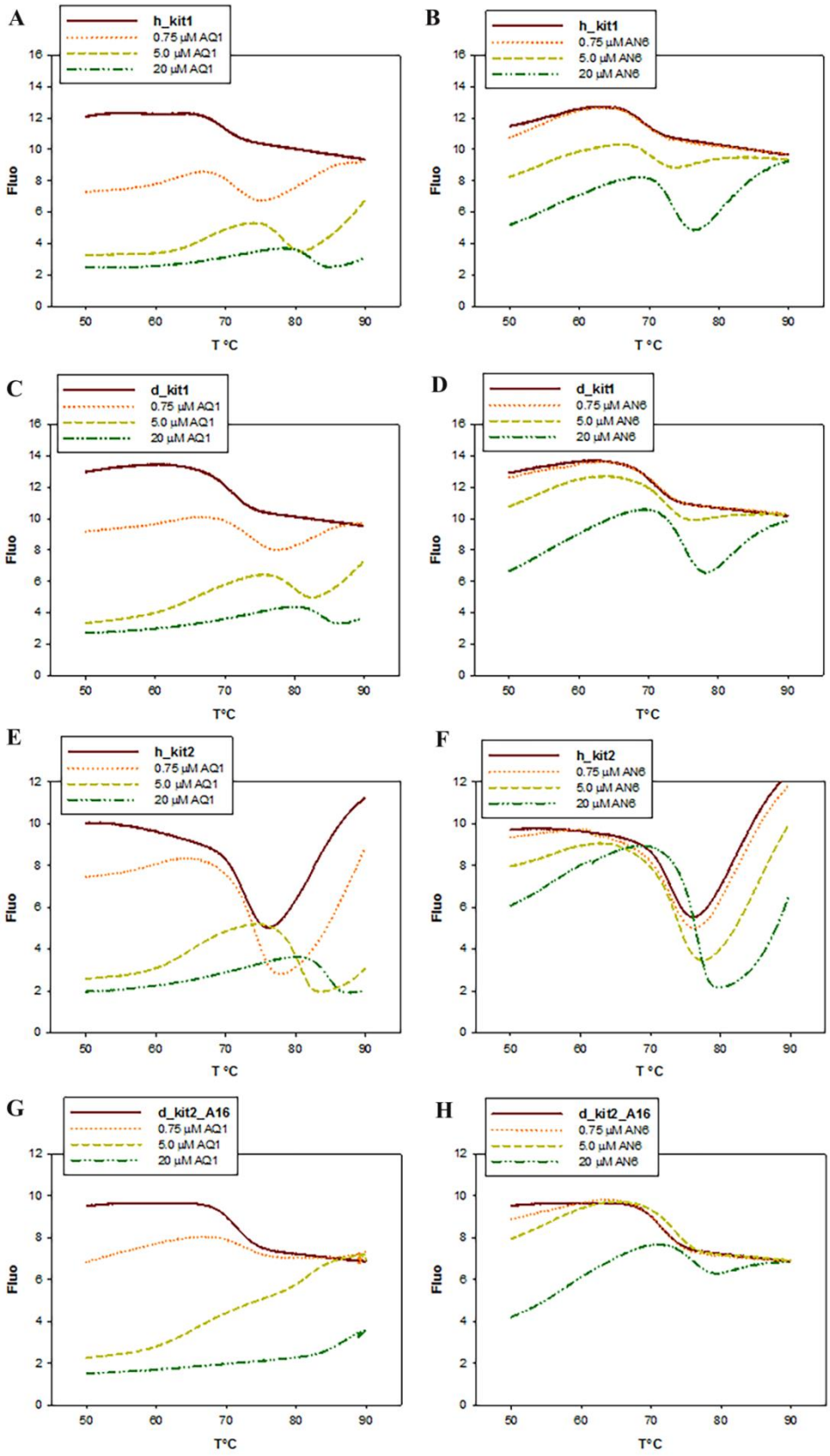

Figure 3

JPET Fast Forward. Published on October 1, 2018 as DOI: 10.1124/jpet.118.248997
This article has not been copyedited and formatted. The final version may differ from this version.

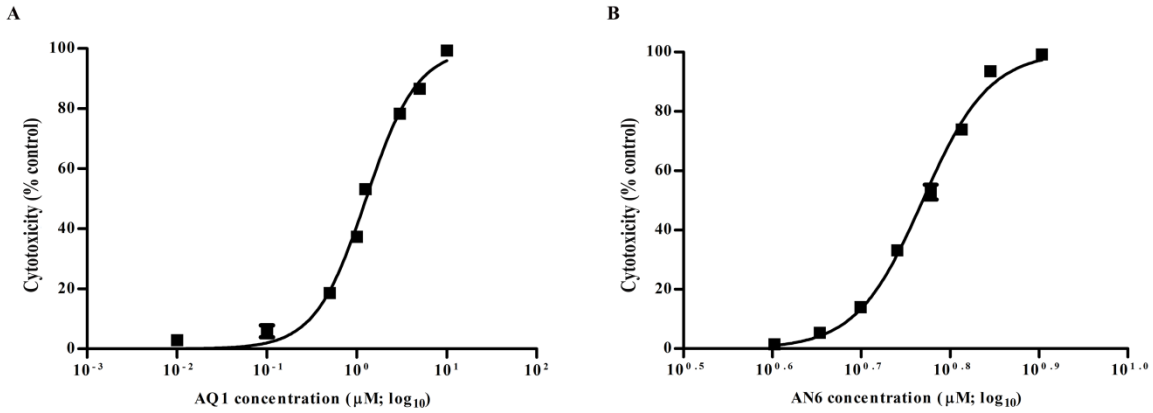

Figure 4

JPET Fast Forward. Published on October 1, 2018 as DOI: 10.1124/jpet.118.248997
This article has not been copyedited and formatted. The final version may differ from this version.

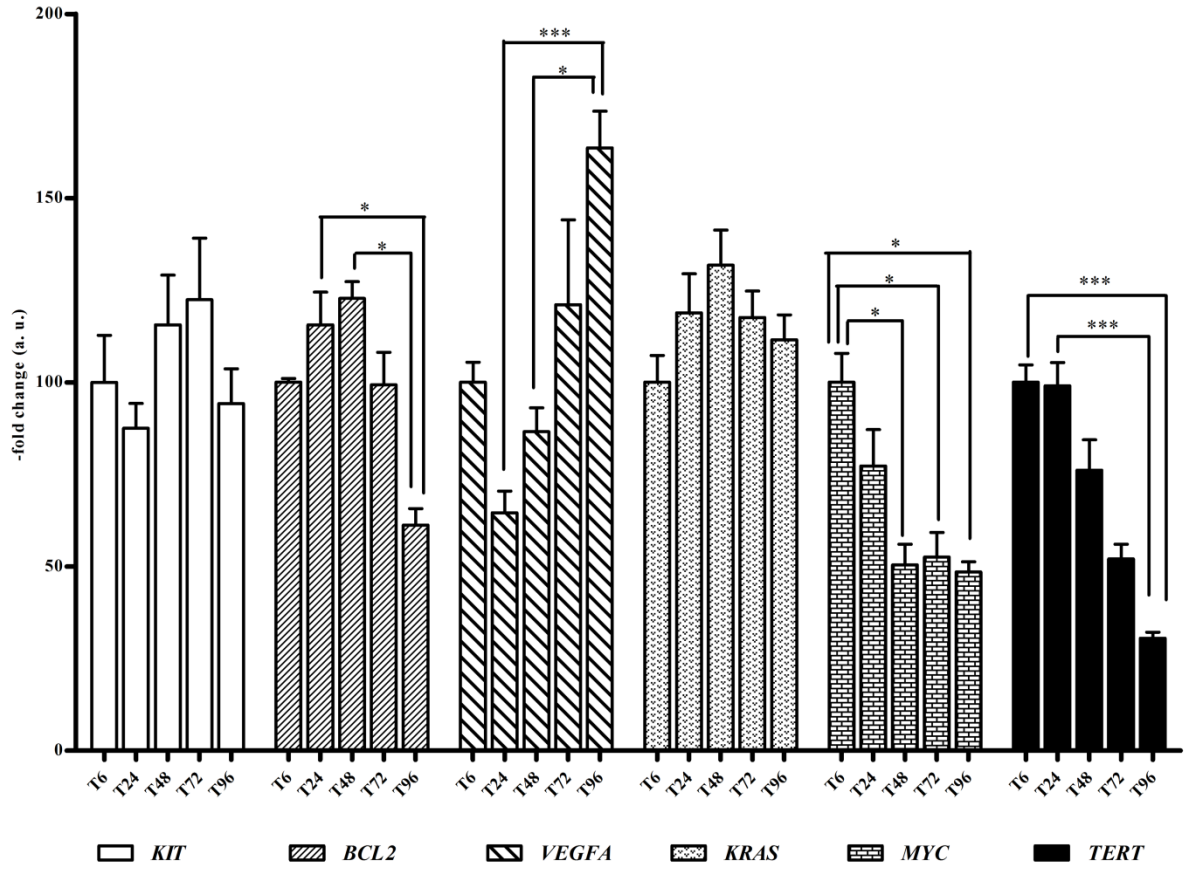

Figure 5

JPET Fast Forward. Published on October 1, 2018 as DOI: 10.1124/jpet.118.248997
This article has not been copyedited and formatted. The final version may differ from this version.

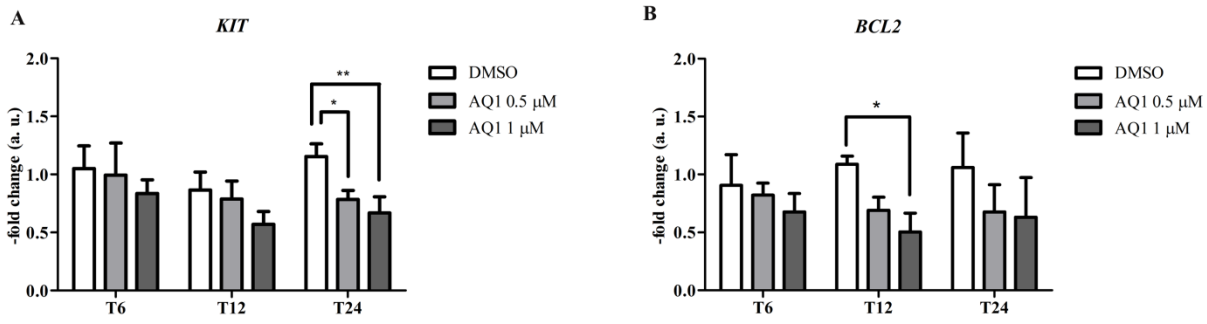

Figure 6

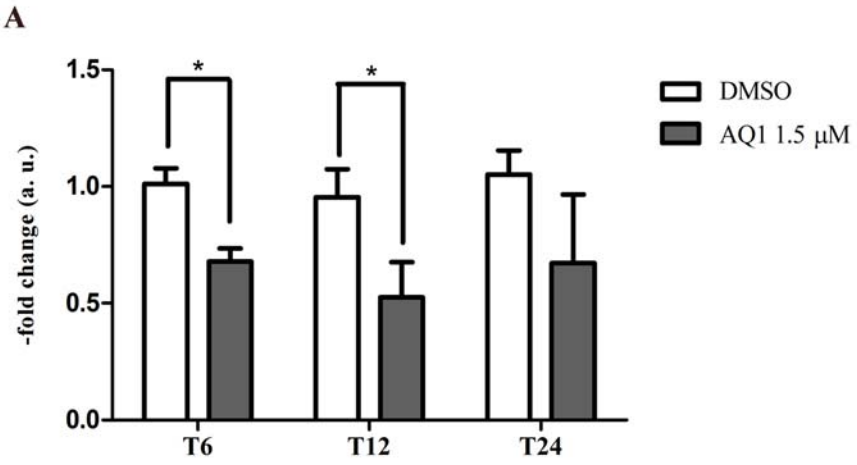

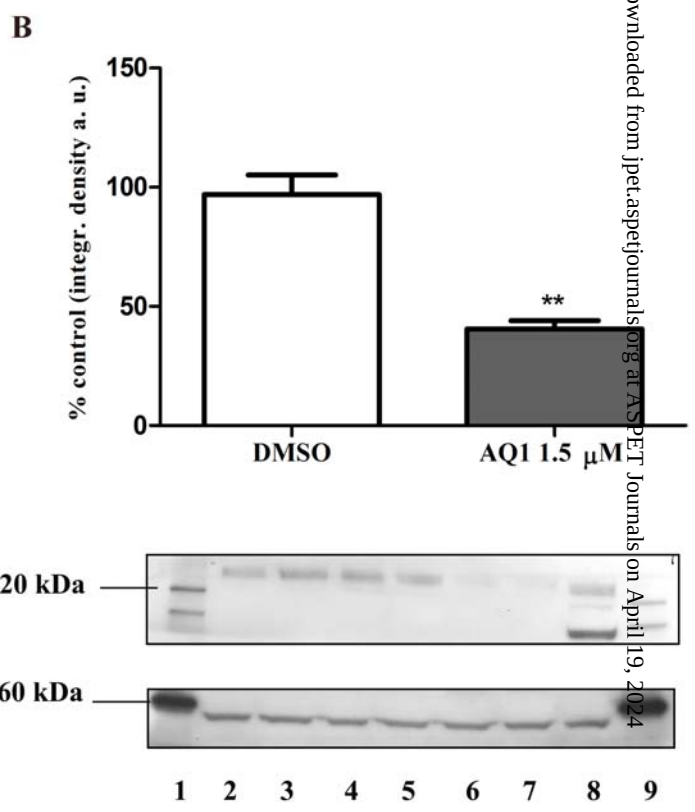

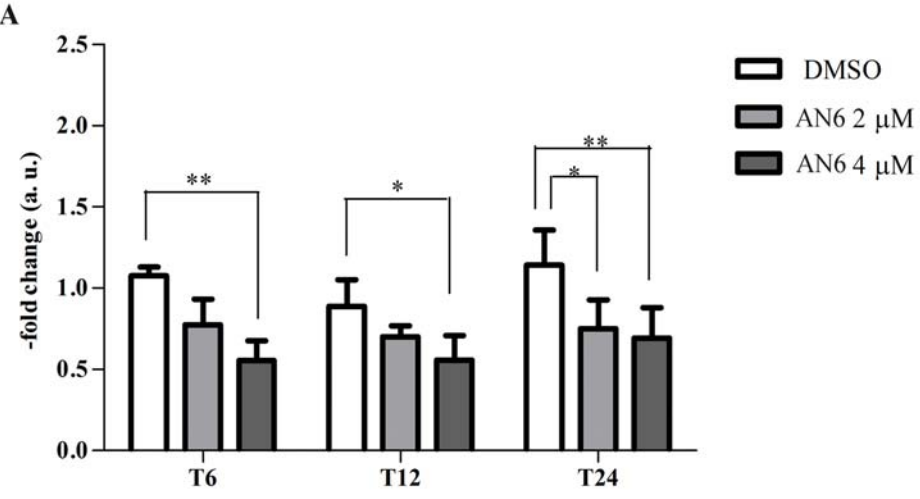

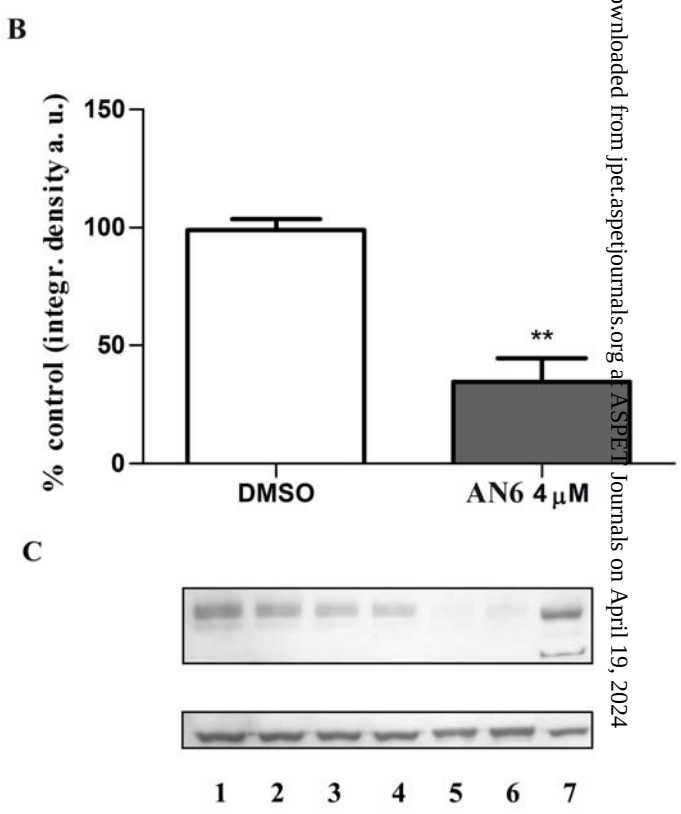

JPET Fast Forward. Published on October 1, 2018 as DOI: 10.1124/jpet.118.248997
This article has not been copyedited and formatted. The final version may differ from this version.

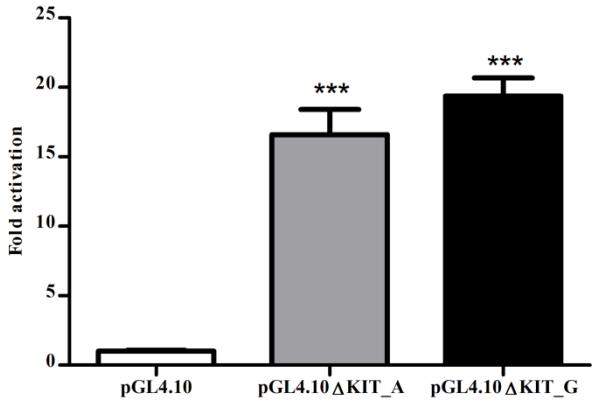

Figure 9

JPET Fast Forward. Published on October 1, 2018 as DOI: 10.1124/jpet.118.248997
This article has not been copyedited and formatted. The final version may differ from this version.

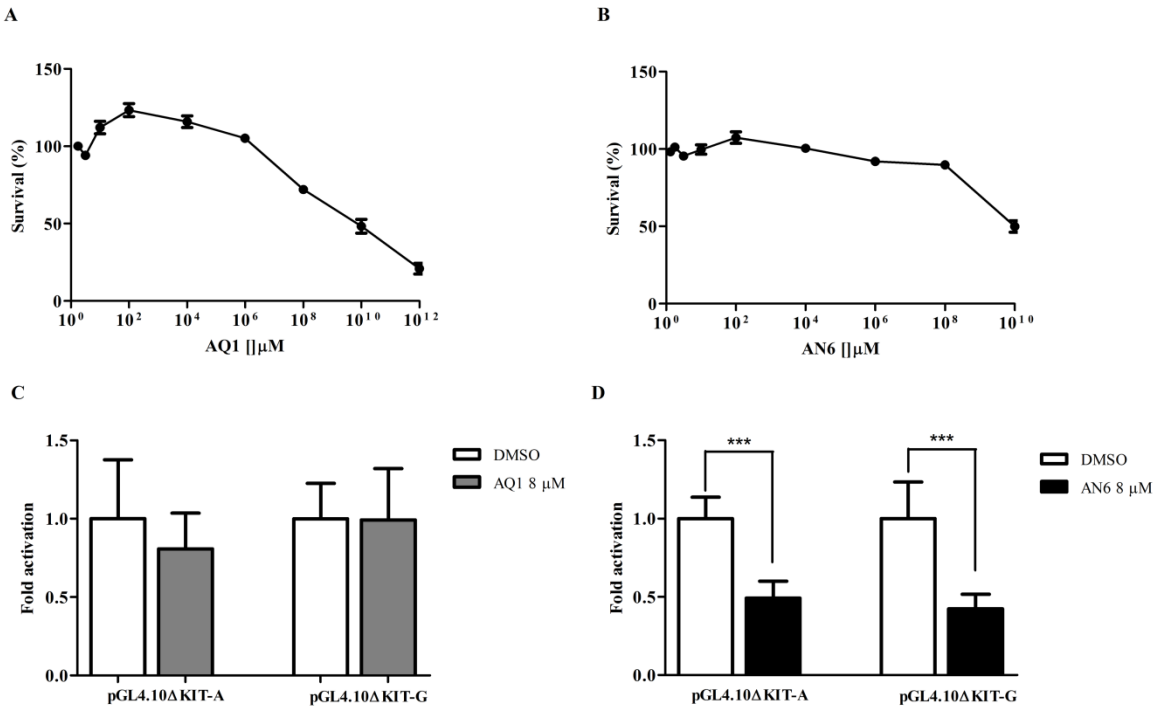

Figure 10